

Selective Surface Metallization of 3D-Printed Polymers by Cold-Spray-Assisted Electroless Deposition

Semih Akin,* Chandra Nath, and Martin Byung-Guk Jun*



Cite This: <https://doi.org/10.1021/acsaem.3c00893>



Read Online

ACCESS |

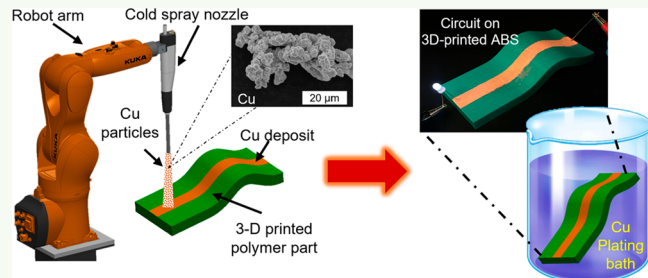
Metrics & More

Article Recommendations

Supporting Information

ABSTRACT: Selective surface metallization of insulating polymers is of particular interest in smart films, energy harvesting, and sensing applications. However, traditional polymer metallization techniques face challenges due to the need for environmentally hazardous pretreatment (e.g., strong acid etching) and cost-intensive palladium seeding processes, thereby limiting the large-scale deployment of metallized polymers. With the advent of rapid prototyping, metallization on additively manufactured polymers drew attention in a variety of technological applications, as it enables the fabrication of low-cost electronic devices. In the current work, we deploy and evaluate a hybrid additive metallization route that can enable the fabrication of functional selective metallization on 3D-printed polymers in a rapid and eco-friendly methodology with improved electrical conductivity. The metallization route sequentially comprises (1) material extrusion 3D printing, (2) cold spray metallization, and (3) electroless deposition. The resulting metal (copper) layers on the polymer surfaces are characterized in terms of the microstructure, surface chemistry, wettability, and electrical conductivity. Notably, selective metallization with promising electrical conductivity (i.e., $6.47 \times 10^6 \text{ S m}^{-1}$ for ABS and $5.27 \times 10^6 \text{ S m}^{-1}$ for PLA parts) is achieved on both linear and curvilinear polymer surfaces. Moreover, strong adhesion between the metallized layer and the 3D-printed structures was confirmed by adhesion tests. Detailed evaluation of the proposed hybrid metallization route unlocks great potential to advance the field of conductive surface metallization on 3D-printed polymers.

KEYWORDS: polymer metallization, polymer electronics, additive manufacturing, 3D printing, cold spray, electroless deposition, electrical conductivity, adhesion strength tests



Downloaded via PURDUE UNIV on September 12, 2023 at 02:27:44 (UTC).
See https://pubs.acs.org/sharingguidelines for options on how to legitimately share published articles.

However, most of the commercial conductive filaments, such as Protopasta, Black Magic, and Electrifi,¹² are poorly conductive (i.e., 3750 times less than a standard bulk copper (i.e., $58.7 \times 10^6 \text{ S m}^{-1}$),⁴ thereby limiting the pragmatic utilization of the resultant products in electronic applications. Moreover, conductive filaments are generally made of carbon black (i.e., brittle and vulnerable material to fracture), which accelerates the wearing of the 3D printer nozzle due to infused carbon fiber strands in the filament.¹²

To address the poor conductivity of the conductive thermoplastic filaments, catalyst-embedded filaments were proposed for 3D-printed parts followed by electroless or electrodeposition.^{13–15} This approach enabled area-selective metallization and led to a significant improvement in electrical conductivity (i.e., $44.4 \times 10^6 \text{ S m}^{-1}$)¹⁵ as compared to the bare

Received: July 4, 2023

Accepted: August 24, 2023

INTRODUCTION

Metallization on polymer materials is becoming attractive for the rational replacement of metals by recyclable and lightweight polymers in various applications as to facilitate energy savings while eliminating or alleviating environmental impacts.¹ In particular, selective metallization on polymer surfaces is of particular interest in the fields of electronics, energy harvesting, sensing, military equipment, automotive industry, aerospace industry, and aesthetic decoration owing to many intrinsic advantages of polymers including their durability, lightweight, impact resistance, design flexibility, and low-cost manufacturing.^{2–4} Conventional approaches used in polymer metallization mainly involve lithography,⁵ vapor deposition,⁶ screen printing,⁷ inkjet printing,⁸ and laser-induced metallization.^{9,10} Despite their own great promises, rapid custom prototyping of conductive patterns on polymers in a facile, eco-friendly, and cost-effective manner remains challenging.

Recently, owing to rapid prototyping of objects through 3D printing techniques, additive manufacturing (AM) approaches using thermoplastic-based conductive filaments have gained much attention, and viable results were achieved.^{11,12}

carbon black filaments. Besides, laser-induced metallization was also proposed to achieve high-resolution conductive patterns on the 3D-printed polymers from Pd-embedded polymers.^{16,17} Nevertheless, Pd is a rare and expensive catalyst material,¹⁸ which can limit the cost-effective and large-scale utilization of these techniques. As an alternative to the Pd seeding, some studies employed conductive pastes (e.g., silver (Ag) paste) followed by electroless deposition (ED) to create structural polymer electronics with high electrical conductivity (42.6×10^6 S m⁻¹).¹⁹ Even though Ag is an excellent seed material (catalyst) to activate the ED process,²⁰ it remains necessary to replace the high cost of Ag-based compounds with a more cost-effective and abundant metal catalyst. Taken all together, these above-mentioned limitations of current manufacturing approaches impede the rapid and large-area metallization of AM-based polymer prototypes, and thus there is a critical need for high-throughput surface metallization methods for 3D-printed polymers made of cost-effective off-the-shelf polymer filaments.

Therein, the emerging cold spray (CS) surface deposition technique would confront the above-mentioned limitations of the current polymer metallization techniques owing to its unique advantages, including low process temperature, high deposition rate, and corrosion resistance.²¹ Owing to these features, CS enables solid-state deposition of micrometer-scale metal particles on polymer surfaces with minimal risk of delamination of the plastic substrates.²² Despite these intrinsic advantages, it remains challenging to achieve electrically conductive metallization through the solely cold spraying of hard metal particles such as copper (Cu) on thermoplastic substrates for polymer electronics applications. The reasons are (i) poor erosion resistance of polymers²³ and (ii) the polymer jetting phenomenon.²⁴ To elaborate, the high-speed bombardment of particles leads to erosions as well as localized melting of the polymer (i.e., jetting) that acts as a separator among the as-deposited particles by encapsulating them.²⁵ Although this phenomenon helps to increase the adhesive strength of CS deposits on polymer substrates, on the other side, it prevents the continuous junction among the particles, preventing the electrical conductivity on the as-CS surface.²⁶

Recently, the authors' group have addressed this issue by developing a CS-based hybrid surface metallization approach, which relies on the integration of the CS and ED processes.^{27,28} In this regard, the as-CS Cu deposits were utilized as the nucleation sites for the subsequent ED (i.e., overplating) process to improve the electrical conductivity on the commercial polymeric substrates.²⁷ Moreover, particle impingement studies on the polyamide (Nylon 6) plates were conducted through numerical modeling to investigate the effect of CS settings on the creation of a catalytic surface for triggering the subsequent ED process.²⁸ Considering recent advances in rapid prototyping technology, the same hybrid metallization approach could synergistically shift the paradigm from an environmentally conscious process (e.g., acid treatment) to an eco-friendly and low-cost process along with many significant advantages, including the making of near-net-shaped parts. Thus, it is of high interest to evaluate and understand such CS-based functional surface metallization on 3D-printed parts for the rapid custom prototyping of polymer electronics.

To this end, the present study aims to adopt the initially proposed CS-based hybrid metallization approach²⁷ for functional surface metallization on 3-D printed freeform ABS and PLA parts. The main objectives of this work are to (1)

establish and adopt a complete additive surface metallization route that enables rapid and eco-friendly metallization of 3D-printed parts in an etching-free manner, (2) perform a fundamental study of the CS-assisted electroless deposition approach, and (3) demonstrate the viability of the proposed route for polymer electronics. The metallization route sequentially involves (i) rapid prototyping of polymer parts through the material extrusion 3D printing, (ii) CS metallization, and (iii) ED processes. First, for rapid prototyping, the material extrusion method is chosen owing to its ease of use, prototyping accuracy, wide range of applications, and low cost.²⁹ Following prototyping by material extrusion, the substrate surface is metallized by the CS process. Lastly, the electroless Cu deposition is performed to ensure high and stable electrical conductivity along the as-CS layer. The resultant functional metallization on 3D-printed parts has been comprehensively studied in terms of microstructure, surface chemistry, wettability, electrical conductivity, and interfacial adhesion strength. Moreover, the electrical performance of the proposed approach is compared to the traditional polymer metallization approaches. To demonstrate the viability of 3D freeform surfaces, metallization on nonplanar geometries is also achieved by multiaxis processing through a programmable robot arm.

EXPERIMENTAL SECTION

Materials. The materials used in this study are given in Table 1. Typical acrylonitrile–butadiene–styrene (ABS) and poly(lactic acid)

Table 1. Materials Used in This Study

process	materials	source
material extrusion 3D printing	ABS, PLA	Sindoh Inc.
cold spray metallization	copper (Cu) particles	Centerline Ltd.
electroless deposition	copper(II) sulfate pentahydrate (CuSO ₄ ·5H ₂ O); ethylenediaminetetraacetic acid (EDTA); sodium hydroxide (NaOH); hydrochloric acid (HCl); potassium ferrocyanide (K ₄ Fe(CN) ₆ ·3H ₂ O); formaldehyde (HCHO)	Sigma-Aldrich

(PLA) filaments (Sindoh Inc.) were used for the rapid prototyping of polymer substrates through the material extrusion 3D printing method. ABS and PLA were considered for three primary reasons: (i) they are the most commonly used polymers for 3D printing applications due to their intrinsic advantages, including cost-effectiveness, recyclability, and composability,^{30,31} (ii) to understand process versatility for polymer types, and (iii) to compare the performance between the types.

Dendrite-shaped copper (Cu) powders (SST, Centerline, Canada), having a size range of 5–45 μm, as shown in Figures 1a,b, were used as the CS feedstock material. Unlike the traditional functional nano inks (e.g., silver paste, \$2580/lb³²), the Cu microparticles used in the present study promise a cost-effective solution (\$30/lb³³) as a functional material for polymer electronics. All chemicals were used as-received without any further purification.

Additive Surface Metallization Route. Figure 2 illustrates the additive metallization route for 3D-printed polymers. First, the polymer substrates (i.e., ABS and PLA) are rapidly prototyped with the material extrusion method. The surface of the polymers is then metallized by the CS deposition, which creates a Cu film on the surface. Lastly, to improve the electrical conductivity, selective conductive metallization on the polymer surface is achieved through the subsequent ED process by utilizing the CS deposits as the active catalytic site. Notably, the proposed route does not require any presurface acid etching to activate the polymer surface; thereby, it is

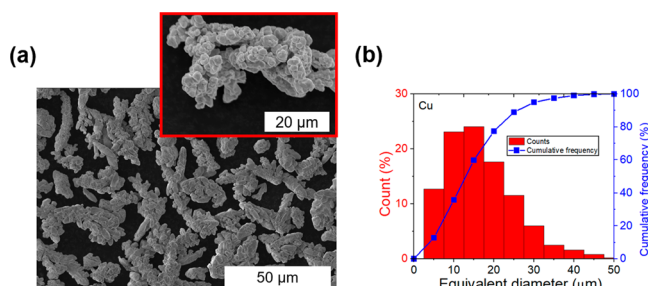


Figure 1. (a) Morphology and (b) size distribution of the feedstock Cu particles.

an environmentally friendly approach for polymer metallization. The following subsections describe each process step of the metallization route in detail.

Material Extrusion 3D Printing. Polymer parts are produced by a common 3D printer (Sindoh 3DWOX) having an orifice nozzle with a diameter of 0.4 mm. The design of the polymer parts was exported as .stl files, and the g-codes were then created from .stl files using the software 3DWOX Desktop. As shown in Figure 2a, the layer-by-layer printing of the ABS and PLA parts (length = 30 mm, width = 20 mm, thickness = 5 mm) was conducted on a heated bed with a temperature of 90 °C (in the case of ABS printing) and 60 °C (in the case of PLA printing) by using a single extrusion nozzle. The settings of the 3-D printing process are listed in Table 2.

Cold Spray Metallization. Cold spray (CS) particle deposition, also known as cold gas dynamic spray or cold spray additive manufacturing, is an emerging solid-state material consolidation technology for rapid metallization on target surfaces owing to its high deposition rate, strong adhesion strength, and low operating temperatures.^{22,25,34,35} In CS, the particle deposition is performed below the melting point of the sprayed feedstock material so that the process can avoid oxidation, minimize thermal degradation, and consume low energy without a need of high-temperature explosive gases and radiation, thereby making the CS as a green and safe surface deposition technology.³⁶ Traditionally, in the CS process, as shown in

Table 2. Process Parameters and Their Settings

procedure	parameter	setting
material extrusion 3D-printing	filament diameter [mm]	1.75
	bed temperature [°C]	90 (ABS), 60 (PLA)
	extruder temperature [°C]	250 (ABS), 200 (PLA)
	layer height [mm]	0.2
	print speed [mm s ⁻¹]	40
	first layer speed [mm s ⁻¹]	1
	driving gas type [-]	air
	driving gas pressure [MPa]	0.7
	driving gas temperature [°C]	80
	powder feed rate [g s ⁻¹]	0.1
CS metallization	nozzle transverse speed [mm s ⁻¹]	75
	spray distance [mm]	10
	number of spray pass [-]	1

Figure 2b, the micrometer-scale metal particles (e.g., copper, tin, zinc, etc.) are accelerated at higher velocities (i.e., 300–1200 m s⁻¹) through a supersonic gas stream.^{21,37} When the particle stream impacts the target, the kinetic energy of particles is absorbed by the substrate surface, leading to high-strength material consolidation due to the metallurgical bonding and/or mechanical interlocking of the particles at particle–substrate interface.³⁸ Unlike the metal substrates, mechanical interlocking (i.e., rigidly embedding of particles into the polymer) is mainly responsible for CS metallization on thermoplastic polymers such as ABS and PLA.²⁵

Accordingly, in this work, micrometer-scale Cu particles were sprayed on the 3D-printed polymer surfaces using a low-pressure CS system (Rus Sonic Technology Ltd., Model K205/407R). The CS system includes an internal gas heater in the spraying gun, an axisymmetric supersonic nozzle, and a powder feeder. The powders were injected into the divergent section of the nozzle. Compressed air

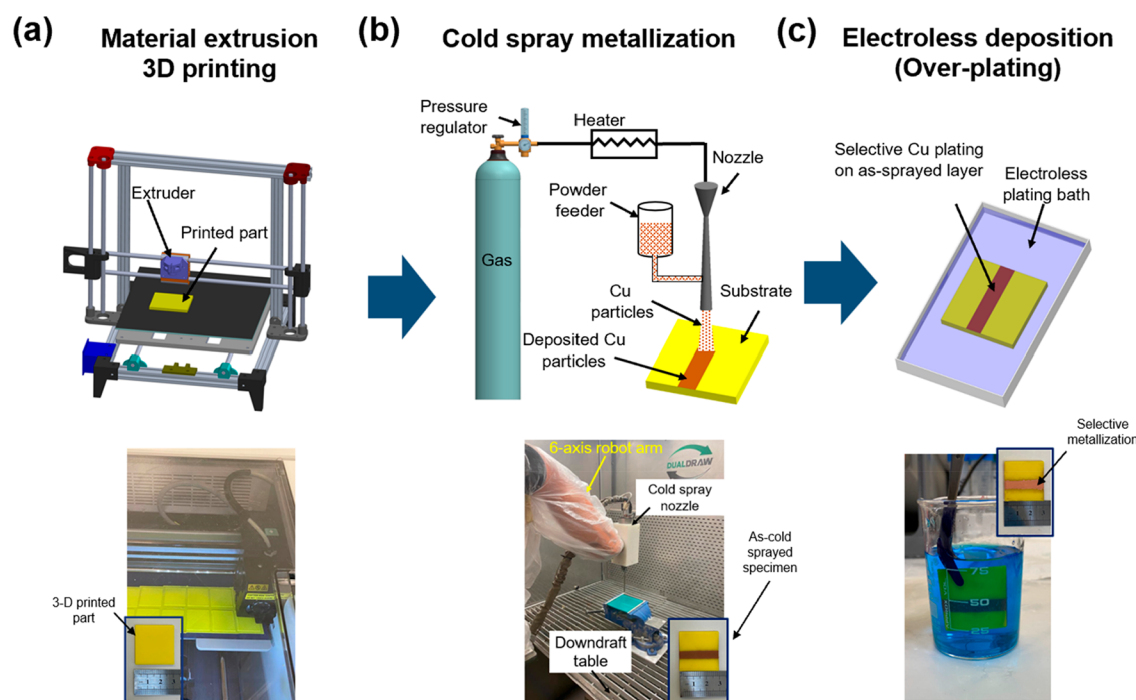


Figure 2. Schematic of the additive metallization route (upper panel) and representative images of each process (bottom panel): (a) material extrusion 3-D printing; (b) cold spray metallization; (c) electroless deposition (overplating).

was used as the process (propellant) gas for the CS process. To precisely control the particle deposition and patterning, the CS gun was mounted on a programmable multiaxis robot arm that enabled metallization on freeform curvilinear polymer surfaces without a need of dedicated mask equipment. The CS settings used in the experiments are listed in **Table 2**. Note that the gas temperature was measured around 80 °C at the nozzle tip using an IR camera (FLIR A300) (Figure S1, Supporting Information). Under these CS settings, the deposition efficiency was calculated at around 12%, which is comparable with the literature.^{39,40}

Electroless Deposition (Overplating). To improve the electrical conductivity, as shown in **Figure 2c**, the ED was subsequently employed as an overplating process by utilizing precold sprayed Cu particles as the nucleation sites. ED was chosen owing to its industrial applicability, eco-friendliness, effective thickness control, high selectivity, high deposition rate, high process throughput, and low cost of materials.⁴¹ The Cu plating bath was prepared by following the recipe described in refs 42 and 43. The composition of the plating bath, with regard to the description, is presented in **Table 3**. To

Table 3. Chemical Composition of the Electroless Copper Deposition Bath

chemical	concentration	description
copper(II) sulfate pentahydrate ($\text{CuSO}_4 \cdot 5\text{H}_2\text{O}$)	18 g L^{-1}	source of Cu^{2+} ions
ethylenediaminetetraacetic acid (EDTA)	48 g L^{-1}	chelating agent
sodium hydroxide (NaOH)	45 g L^{-1}	pH controlling agent
potassium ferrocyanide ($\text{K}_4\text{Fe}(\text{CN})_6 \cdot 3\text{H}_2\text{O}$)	200 mg L^{-1}	stabilizing agent
hydrochloric acid (HCl)	18 mL L^{-1}	leaching agent
formaldehyde (HCHO)	15 mL L^{-1}	reducing agent

constitute the plating bath, the chemicals are dissolved in deionized water (1 L L^{-1}) followed by the addition of the reducing agent (formaldehyde). The plating process was conducted at room temperature by setting the pH value of the bath around 12. Various plating times (i.e., 0.5–3 h) were applied to the as-CS specimens to investigate the effect of ED time on the deposition morphology, film thickness, and electrical conductivity.

Characterization. Scanning electron microscopy (Hitachi S-4800) and optical microscopy (AMScope) were used to analyze the microstructure of the resultant metallization. The chemical composition of the resultant metal layers was characterized by energy-dispersive X-ray (EDX) analysis using the same Hitachi S-4800 equipment. Moreover, X-ray diffraction (XRD) measurement was also conducted to investigate the crystalline structure of the as-CS and overplated surfaces. The water contact angle measurements of the samples were conducted based on the sessile drop technique.⁴⁴ The surface roughness of the specimens was quantified by a surface roughness tester (AMTAST). A digital multimeter (Agilent/HP 34401A) was used to measure the resistance of the resulting metallization. Moreover, the sheet resistance (R_s) of the fabricated electrodes was measured using a 4-point probe system (Jandel, RM3-AT) at a constant current of 100 mA. The Scotch (3M magic tape) tape test method was applied to investigate the adhesion strength of the metallized layers.⁴⁵ Besides, the ASTM D3359-02 standard tape test⁴⁶ and ASTM D4541 pull-off adhesion test⁴⁷ were conducted to quantify the interfacial adhesion strength between the deposited metal film and the polymer substrate. All the characterizations were performed at room temperature by considering $n = 3$ specimens for each characterization test.

RESULTS AND DISCUSSION

Characterization of Deposition Morphology and Microstructure. **Figure 3** shows digital images of the as-CS ABS and PLA surfaces under the same CS settings in **Table 2**.

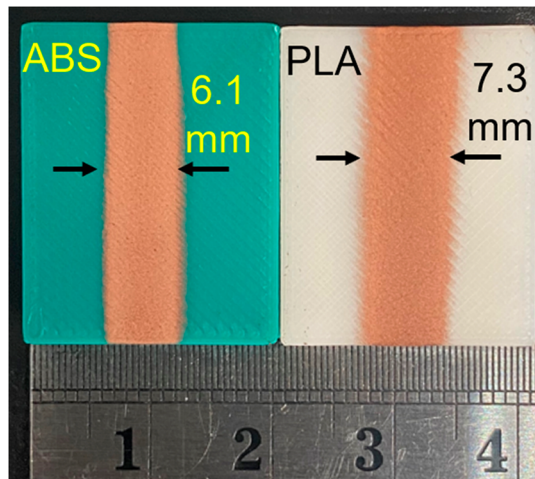


Figure 3. As-CS Cu traces on 3D-printed ABS (left panel) and PLA (right panel) parts.

Interestingly, after the CS process, it was observed a difference in line width between the polymer types. In detail, larger line width (i.e., $\approx 20\%$ larger) was observed for the PLA parts as compared to the ABS specimens. The difference in CS line width between the polymer types is likely attributed to the distinct adherence mechanism of the Cu particles on the polymer types due to the thermal softening phenomenon.⁴⁸ The thermal softening temperature of the PLA is less (i.e., 36% less) than that of the ABS parts. Given that the softening temperature of PLA is around 60 °C⁴⁹ (i.e., less than the temperature measured by the nozzle as shown in **Figure S1**), the impinging particles could experience more dispersion onto the PLA surface, resulting in a CS deposition with a relatively larger line width as compared to the ABS parts.

As for the microstructure analysis shown in **Figure 4**, the surfaces of both polymer types were successfully metallized through the CS process, having an average Cu film thicknesses of approximately 43 μm (ABS) and 56 μm (PLA), respectively. The difference in film thickness between the ABS and PLA parts could be attributed to the lower impact strength of the PLA as compared to the ABS⁵⁰ (i.e., 7 kJ/m^2 for PLA against 42 kJ/m^2 for ABS filaments in this study⁵¹). In detail, the CS particles impinged deeper into the PLA substrate due to its lower impact resistance, resulting in a thicker CS metallization than that of the ABS parts.

Figure 4c presents the SEM analysis of the as-CS ABS surface. The local porosities ($\approx 30\%$; see **Figure S2**) were observed on the surface, which is primarily attributed to spatial erosion and polymer jetting of the polymer surface due to the high-speed impingement of the Cu particles.⁵² Moreover, several discrete polymer regions locally appeared on the as-CS surface, which can be seen from the highlighted spots in **Figure 4c**. Given the interactions between the particles and the polymer substrate primarily occur in the initial steps of the CS deposition,⁴⁸ the localized high-strain rate deformations of the polymer substrate encapsulate the embedded particles.⁵³ These localized deformations might act as a separator among the as-CS Cu particles, thereby preventing homogeneous electrical conductivity. The EDX analysis in **Figure 4d** also confirmed the existence of the localized polymer regions on the resulting deposit by presenting a remarkable amount of carbon (C) element on the as-CS surface. Besides, **Figure 4e–g** demonstrates that the as-CS PLA parts exhibited a comparable

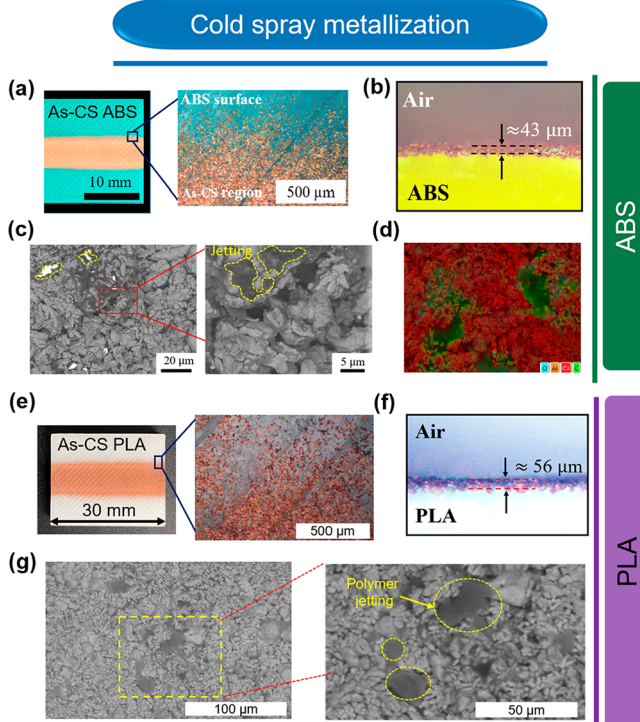


Figure 4. (a) Digital and OM images of the as-CS ABS surface. (b) Cross-sectional image of the as-CS ABS. (c) SEM image of the as-CS ABS surface. (d) EDX map of the as-CS ABS surface. (e) Digital and OM images of the as-CS PLA surface. (f) Cross-sectional image of the as-CS PLA. (g) SEM image of the as-CS PLA surface.

surface microstructure to the as-CS ABS. This similarity is characterized by localized porosities across the surface and interface, attributed to the high-speed impingement of Cu particles into the PLA substrate.

On the other hand, as shown in Figure 5a, the subsequent ED filled the porosities and voids among the embedded Cu particles on the ABS surface. After a 3 h ED, the resulting film thickness was measured around 53 μm for ABS (Figure 5b), revealing that about 10 μm thick Cu film was formed by the ED process. SEM images in Figure 5c also justified the formation of a continuous Cu film on the overplated ABS. Furthermore, the ED analysis confirmed the homogeneous distribution of the Cu elements on the overplated surface (see Figure 5d). The ED also successfully created a Cu overlayer on the as-CS PLA parts as shown in Figure 5e, having a microstructure comparable to that of the overlaid ABS parts. The overall film thickness was obtained as 68 μm (Figure 5f), indicating that nearly 12 μm thick Cu film was created by the 3 h ED process. Notably, as seen in Figure 5g, the ED process led to the formation of a complete Cu film on the PLA surface by covering the jetted regions on the as-CS PLA surface (Figure 4g). As such, the ED process ensures a continuous and homogeneous conductive path along the as-CS traces for both polymer types. However, several local porosities were observed along the cross-section of the overplated specimens (see Figure S3). It indicates that even though a thin film of homogeneous Cu deposit is achieved on the as-CS surface, the ED cannot ensure a fully covered metal film along the interface of the polymer substrates.

Lastly, as shown in Figure 6, XRD measurements were conducted to characterize the composition and crystalline

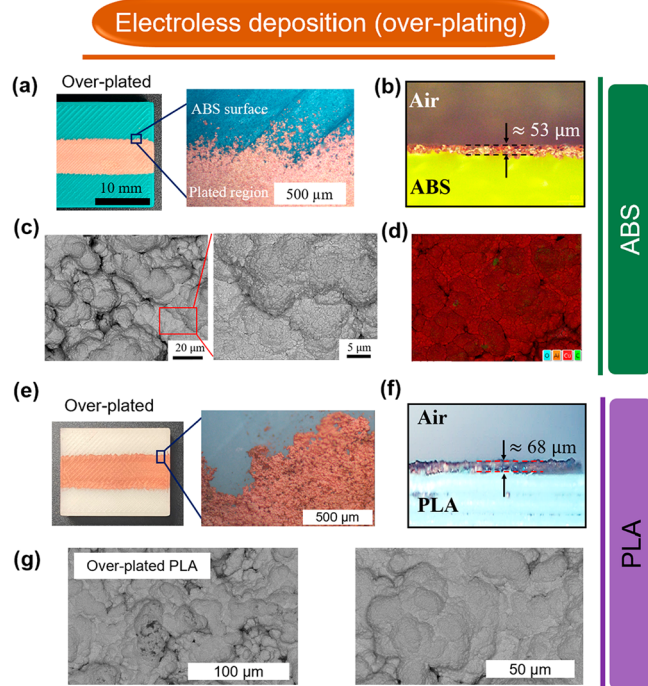


Figure 5. (a) Digital and OM images of the 3 h ED ABS surface. (b) Cross-sectional image of the 3 h ED ABS. (c) SEM image of 3 h ED ABS surface. (d) EDX map of the 3 h ED ABS surface. (e) Digital and OM images of the 3 h ED PLA surface. (f) Cross-sectional image of 3 h ED PLA part. (g) SEM image of the 3 h ED PLA surface with different image resolutions.

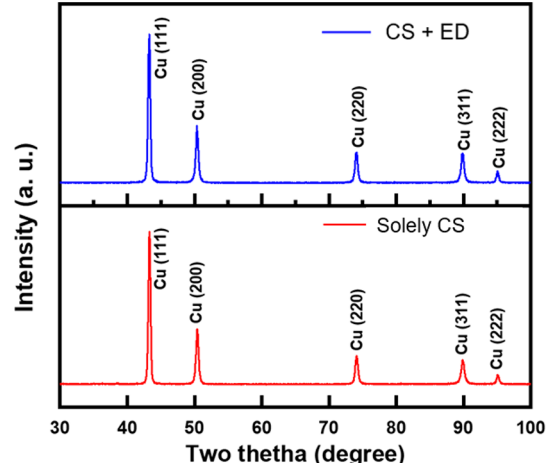


Figure 6. XRD spectrograph of the as-CS (bottom panel) and 3 h ED ABS surface (top panel).

structure of the as-CS and the ED surfaces in the 2θ angle range of 0–100°. The Cu peaks in both as-CS and ED surfaces appeared at $2\theta = 43.3^\circ$, 50.5° , 74.2° , 89.9° , and 95.1° , representing (111), (200), (220), (311), and (222) planes, respectively. No additional strong peaks appeared in the XRD patterns of the overplated ABS surface, which represents a high purity for the fabricated Cu deposit. No extra peaks were detected in these examinations, revealing that the crystalline structure of Cu particles is preserved during the ED.

Wettability Analysis. The wettability characteristics of the specimens, as shown in Figure 7 and Table 4, were investigated by considering the water static contact angle (CA) at various

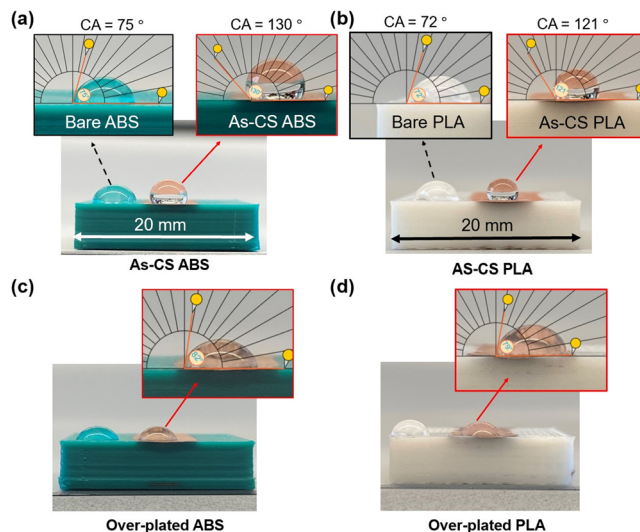


Figure 7. Surface wettability characteristics of (a) bare (top left) and as-CS (top right) ABS, (b) bare (top left) and as-CS (top right) PLA, (c) 3 h ED ABS, and (d) 3 h ED PLA specimens.

Table 4. Surface Roughness and Contact Angle Data of the Specimens

material	specimen	R_a (μm)	contact angle (deg)
ABS	bare (neat)	3.59 ± 0.75	75 ± 5
	as-cold sprayed	4.48 ± 0.32	130 ± 7
	overplated	3.47 ± 0.33	77 ± 5
PLA	bare (neat)	2.85 ± 0.74	72 ± 7
	as-cold sprayed	3.91 ± 0.42	123 ± 8
	overplated	3.24 ± 0.28	74 ± 6

surface conditions: (i) bare 3D-printed polymer, (ii) as-CS, and (iii) overplated surfaces. The water droplets were dropped at distinct locations on the polymer surfaces to observe the static behavior of the droplets. As shown in Figure 7a,b (left panel), the average CA of the bare polymer surfaces was measured at 75° (in the case of ABS) and 72° (in the case of PLA). The CA significantly increased after CS, resulting in a wetting transition from hydrophilic (i.e., $\text{CA} < 90^\circ$) to hydrophobic (i.e., $\text{CA} > 90^\circ$) (see Figure 7a,b, right panel). It is likely attributed to the resulting microrough surface structure due to the impinging particles onto the polymer substrate during CS (see Figures 4a and 5a) that decreased the contact area between the sessile drop and the as-CS surface.

There are mainly two mechanisms that are responsible for the hydrophobic properties of the coatings, which are (i) surface energy (i.e., chemical composition of the surface) and (ii) surface topography (i.e., surface roughness).⁵⁴ For the surface topography, the CA is generally increased on rough surfaces according to the relationship between the surface roughness and contact angle as described by the Wenzel and Cassie–Baxter relations.⁵⁵ Table 4 shows the surface roughness values measured in the axial direction along the metallized layers (Figure S4). The as-CS specimens resulted in higher roughness than the bare polymer parts, which increased the hydrophobicity of the polymer surface. Moreover, the water droplet likely stayed on the metallized layer peaks above the surface entrapping as stated in Cassie–Baxter wetting state,⁵⁶ which can lead to shrinkage of the droplets, resulting in a larger CA. Besides, previous studies reported that the hydrophobic performance of the as-CS surfaces is also attributed to the

hierarchical architectures of the dendrite-shaped feedstock Cu powders.⁵⁷ Overall, in the present study, CS with dendrite-shaped Cu particles (Figure 1a) increased the hydrophobic properties of the polymer surface.

Conversely, as presented in Figure 7c,d, CA sharply dropped into the hydrophilic region after the ED process. The main reason is likely the topography changes during the ED process. In detail, ED filled the porosities on the as-CS surfaces (see Figure 5c,g) and formed a continuous Cu film over the as-CS layer, which alleviated the microroughness of the sprayed layer, thereby decreasing the CA based on the Wenzel model.⁵⁵ As seen in Table 4, the average surface roughness decreased after ED, presenting a less rough surface than the as-CS surface. Moreover, the overplated film would impede the intrinsic hydrophobic properties of the dendrite-shaped as-CS Cu particles by forming a thin metal film on the particles, resulting in a lower CA. It was also reported in refs 58 and 59 that longer ED increases the grain size of the Cu particles, leading to larger surface energy with lower CA (i.e., higher wettability). Overall, solely CS led to a hydrophobic surface, while ED generated a hydrophilic property on the fabricated electrodes.

Electrical Performance. Figure 8a illustrates the corresponding electrical resistance of the resulting polymer metallization at various overplating times for the test units (i.e., conduction path in a size of $\approx 6 \text{ mm} \times 30 \text{ mm}$). As seen in Figure 8a, the electrical resistance decreases with an increase in ED duration. However, the trend of the resistance change is not linear throughout the ED process. In detail, the electrical resistance sharply decreases at the initial stage of 1-h ED, and then it gradually decreases at a slower rate. This apparent decrease in the electrical resistance is attributed to (i) good catalytic properties and (ii) microrough morphology ($R_a = 3.9\text{--}4.5 \mu\text{m}$) of the as-CS surface, which are crucial to trigger the ED process.^{2,60} After 3 h of ED, the resistance reached a plateau around $76 \text{ m}\Omega$ for the ABS and $65 \text{ m}\Omega$ for the PLA specimens, respectively.

It was interestingly observed that the PLA parts showed lower electrical resistance than the ABS parts during the ED process. The difference in electrical resistance for the metallized polymers likely lies in (i) the as-CS film thickness and (ii) the distinct chemical properties of the ABS and PLA parts. To elaborate, the as-CS Cu particles impinged deeper into the PLA part due to its lower impact resistance, thereby increasing the active catalytic surface area for the ED process. Moreover, PLA parts have inherently lower chemical resistance as compared to ABS parts,⁶¹ which could also help to catalyze the ED process. As such, a relatively thicker Cu film was overplated on the as-CS PLA parts as compared to the as-CS ABS.

On the one hand, for both polymer types, there is a quasi-linear relationship between the ED time and film thickness, having a deposition rate of nearly $3.5\text{--}4 \mu\text{m/h}$ (see Figure 8b). It is attributed to the continuing plating reaction under the existence of the reducing agent (i.e., formaldehyde) in the plating path. Because of the autocatalytic nature of the ED process, the deposition takes place until the reducing agent is completely oxidized. Note that the electrical conductivity is not significantly improved by the ED process once a continuous metal layer is formed on the substrate surface,⁶² which can be also seen in Figure 8a. As for the electrical stability, the relative resistance (R/R_0) of the resulting metallization marginally increased along with a storage period of 10 days and then remained almost stable. This could be explained by the

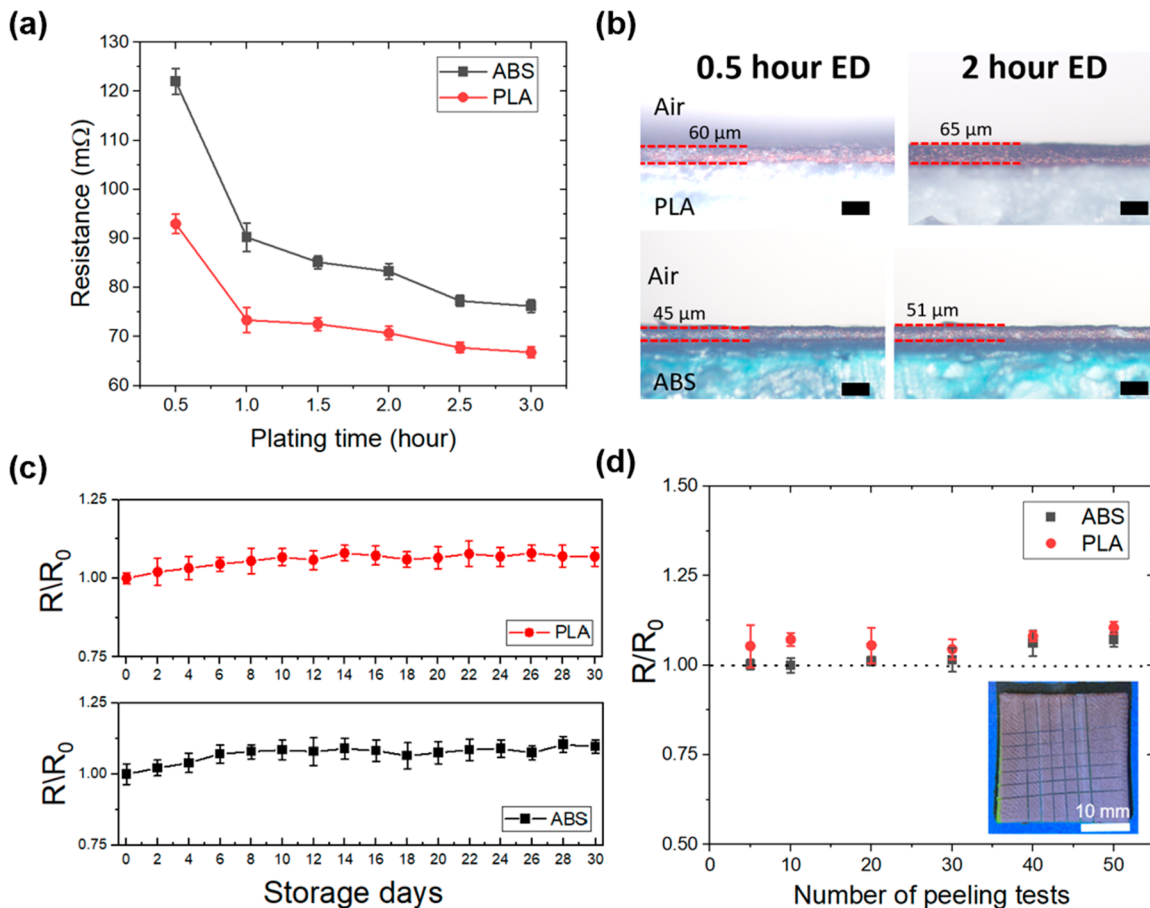


Figure 8. (a) Electrical resistance and (b) film thickness change of the metallized 3D print polymers with different ED times (scale = 100 μm). (c) Relative resistance (R/R_0) change of the resulting metallization (CS+ED) with storage days. (d) R/R_0 change of the resulting metallization under a various number of peeling test cycles.

formation of the oxide layer on the ED surface over storage time.²

Lastly, the electrical conductivity of the fabricated electrodes was calculated by eq 1, where σ is the conductivity (S m^{-1}), ρ is the resistivity ($\Omega \cdot \text{m}$), L is the length (m), R is the electrical resistance (Ω), w is the width (m), and t is the film thickness (m) of the electrode. For the conductivity calculation, the overplated Cu film thickness was considered because electrical conductivity primarily comes from the ED process rather than the as-CS layer. After 3 h ED, the resistance was obtained as 76 mΩ (for ABS) and 65 mΩ (for PLA) based on the two-point probe measurements (see Figure 8a). The widths of the electrodes are 6.1 mm (ABS) and 7.3 mm (PLA), while the length is 30 mm for both electrodes. The film thicknesses after 3 h ED are found to be 10 μm (ABS) and 12 μm (PLA), respectively. By incorporating these features into eq 1, the conductivity (σ) of the fabricated electrodes on the 3-D printed ABS and PLA parts was calculated as 6.47×10^6 and $5.27 \times 10^6 \text{ S m}^{-1}$, respectively. These values show a promising electrical conductivity (i.e., bulk conductivity of copper $\cong 59.6 \times 10^6 \text{ S m}^{-1}$) for the utilization of the resulting functional metallization in various electronic applications.

$$\sigma = \frac{1}{\rho} = \frac{L}{Rwt} \quad (1)$$

Performance Comparison with Traditional Polymer Metallization Approaches.

By considering the electrical

conductivity and sheet resistance, we compared the electrical performance of the proposed route (i.e., CS-assisted ED) with the widely used polymer metallization techniques in the field of polymer electronics. As seen in Table 5, the additive metallization route in this study is found to be promising for electrical conductivity compared to the traditional polymer metallization methods that include acid-etching and material extrusion with conductive filaments. Notably, the proposed approach exhibited about 155-fold higher electrical conductivity over the conventional acid-etching-based metallization approaches (i.e., chemical etching + electroless deposition). Moreover, the proposed approach showed better performance (i.e., ≈ 2.3 -fold for ABS and 3.2-fold for PLA) than the method where the acid etching and electroplating are sequentially comprised.⁶³ The reason lies in the successful CS deposition on the 3D-printed polymer surfaces, which synergistically catalyzed the surface for the subsequent ED process, resulting in highly conductive metallization along the as-CS layer.

Although the proposed metallization route performed lower than the laser-structured metallization technique in terms of electrical performance, the method in this study would enable high-throughput metallization with large-area applicability over the laser-induced metallization techniques. In detail, Cu electrodes with a line width of more than 6 mm can be successfully patterned on the 3D-printed parts by a single CS pass. In addition, as per the application requirements, the

Table 5. Comparison of Various Polymer Metallization Methods Used in Polymer Electronics

metallization methods	substrate	sheet resistance (ohm/sq)	conductivity ($\times 10^6$ S m $^{-1}$)
present study	ABS	0.00433	6.47
present study	PLA	0.00312	5.27
material extrusion with conductive filaments (Protopasta) ¹²	PLA	NA	0.0000083
material extrusion with conductive filaments (Black Magic) ¹²	PLA	NA	0.000128
material extrusion with conductive filaments (Electrifi) ¹²	PLA	NA	0.0071
material extrusion with conductive filaments + Cu plating ⁴	PLA	NA	0.376
chemical etching + electroless deposition ⁶⁸	ABS	0.102–0.23	0.015–0.0338
chemical etching + electroplating ⁶⁸	ABS	0.01–0.02	NA
chemical etching + Al seeding + Cu plating ⁶⁹	ABS	0.1	NA
photolithography ⁷⁰	PolyFlex	0.139	NA
inkjet printing ⁷¹	polyimide film	NA	0.016
screen printing ⁷²	PET	160	0.000714
vapor deposition ⁷³	PEDOT	NA	0.0348
laser-direct metallization ⁷⁴	PC/ABS blend	0.02–0.1	NA
laser-direct metallization ⁷⁵	polyimide film	0.02	NA
laser-direct structuring ¹⁷	UV-curable resin	NA	13.33
laser-direct structuring ²	polymer composite	NA	12.2
comparison with the commercially available polymers having a conductive coating on it			
polymer		sheet resistance (ohm/sq)	
present study (ABS)		0.00433	
present study (PLA)		0.00312	
ITO-PET ⁷⁶		60	
ITO-PEN ⁷⁶		15	

electrical conductivity of the electrodes can be tuned by applying various ED times. Taken together, the CS-based metallization route in this study promises great potential for rapid prototyping and the large-scale production of 3D-printed polymer electronics.

Besides, the electrical performance of the resulting metallization was compared with those of commercial indium–tin oxide-coated poly(ethylene terephthalate) (ITO-PET) and poly(ethylene naphthalate) (ITO-PEN). As seen in Table 5 (bottom panel), the fabricated metallization on the 3D-printed ABS and PLA parts exhibited significantly lower sheet resistance as compared to the commercial ITO-PET and ITO-PEN polymers. Considering ITO is a rare, high-cost, and brittle coating material,⁶⁴ the functional metallization achieved by the proposed route in this study could be a potential alternative to these cost-intensive materials. Besides, owing to the antifouling characteristics of Cu-based coatings,²⁵ the resulting metallization on 3D-printed parts could be also used against detrimental fouling organisms to protect the structures from biological fouling. Furthermore, given the Cu deposits are utilized to create antibacterial and antiviral surfaces, for

example, protecting against the recent global COVID-19 viruses,^{65,66} the fabricated Cu surfaces on the 3D-printed parts can be potentially used as multifunctional (conductive + antiviral) surfaces in polymer electronics, which would be an additional benefit of the proposed metallization route.

Adhesion Strength. Figure 8d shows the relative resistance (R/R_0) change of the resulting metallization (CS + ED) under a number of peeling test cycles using Scotch tape (3M Magic tape). No substantial difference in R/R_0 was observed for the as-plated samples, which confirms the interfacial adhesion between the metallized layer and the 3D-printed polymer surface. Moreover, the cross-cut adhesion test was conducted by evaluating the percent area removed according to the ASTM D3359-02 standard by the ASTM tape test scale.⁶⁷ The details regarding the cross-cut adhesion test are provided in Figure S5. No noticeable peeling or removal was observed on the crosscuts after peeling the tape (Figure S5e), which reveals strong adhesion strength (i.e., the score of SA based on the ASTM D3359-2 test scale) of the fabricated electrodes.

Besides, to evaluate the adhesive strength between the 3D-printed substrate and the fabricated Cu film, pull-off adhesion tests were conducted using a pull-off tester (Elcometer 506). The details of the pull-off test procedure are provided in the Supporting Information (see Figure S6). In each test, the dolly was gradually pulled, and the polymer surface started peeling-off with a strength of around 1.8 MPa. Notably, no delamination was observed for the Cu film at this point. When the test was continued, the surface of the 3D-printed polymer was observed to be locally fractured (see Figure S6c), which eventually resulted in substrate failure (Figure S6d). As such, the results indicate that the bond strength of the deposited Cu film is higher than the intrinsic strength of the 3D-printed polymer surface.

To quantify the adhesion strength of the resulting metallization, further pull-off tests were conducted by employing a commercial ABS plate (ePlastics) with a thickness of 6 mm. The adhesion strength of the fabricated metallization (CS + ED) was measured as 2.84 ± 0.17 MPa, resulting in a complete detachment of the Cu deposit from the polymer surface (Figure S7). Overall, the qualitative and quantitative adhesion test results confirmed the interfacial adhesion between the fabricated metallization and the polymer substrate for polymer electronics applications.

Applications and Prospects. To demonstrate the effectiveness of the metallization route for polymer electronics, a light-emitting diode (LED) blinking circuit was designed on various linear (2-D) and curvilinear-shaped printed parts (3D). First, as shown in Figure 9, a 3D-printed polymer (PLA) puzzle was designed, and a conductive path was fabricated on it. The male sockets and the top surface of the puzzle pieces (see Figure 9a, left panel) were cold sprayed by the robot arm, while the female key sockets (Figure 9a, right panel) were coated by hand-held spraying owing to the portability of the low-pressure CS setup. Subsequently, the puzzle pieces were selectively metallized by the ED to achieve electrical conductivity along the as-CS sections (Figure 9b). Upon assembling the puzzle pieces, the circuit is completed, forming a continuous conductive path (see Figure 9c), which lights up the LED. Considering rapid prototyping approaches that enable cost-effective modular assembly by minimizing/eliminating such special joints between the parts, the metallization route in this study could be valuable not only

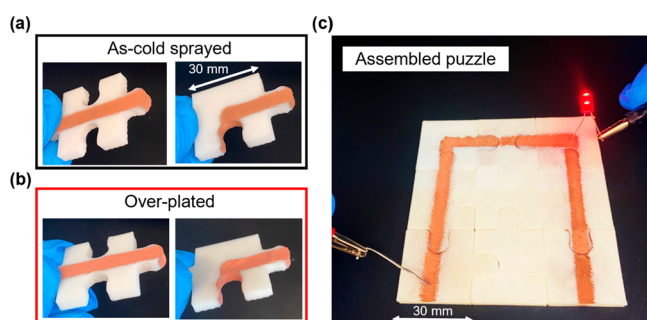


Figure 9. (a) As-CS and (b) overplated puzzle pieces made of PLA filaments. (c) Assembled puzzle with a conductive path.

for functional metallization on 3D-printed parts but also for smart and integrated assembly to constitute 3D-printed integrated circuits. Moreover, such 3D-printed puzzles with conductive paths could be potentially utilized for educational purposes to promote the fundamental understanding of kids toward rapid prototyping and electronic circuits.

The proposed route was also applied for functional metallization on 3D-printed freeform curvilinear surfaces through a programmable robot arm. As shown in Figure 10, conductive metallization on curvilinear-shaped ABS and PLA parts was successfully performed in two different part geometries (dome and convex-concave curvature). Upon

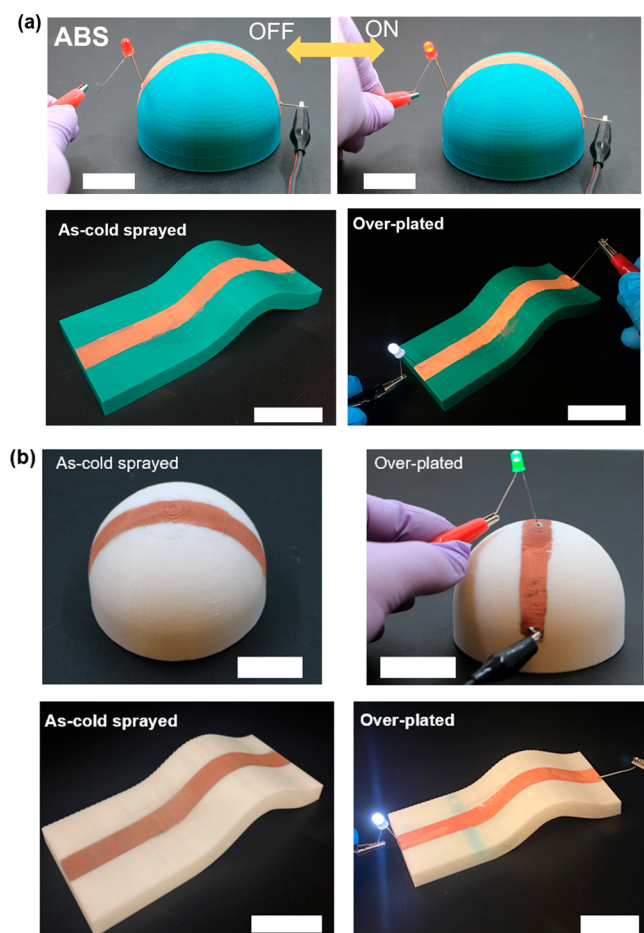


Figure 10. Dome-shaped (upper panel) and convex-concave-shaped (bottom panel) conductively metallized (a) ABS and (b) PLA parts (scale bar = 20 mm).

testing, it is observed that the resulting metallization maintained its same level of conductivity throughout a long conduction path (i.e., >50 mm) without compromising structural integrity. The results reveal that the proposed metallization route can be appropriately used in large-area metallization on curvilinear-shaped 3D-printed polymers owing to its high-throughput multiaxis processing capability without a need of dedicated vacuum equipment. Moreover, because of the robotic arm programming, the kinematic parameters of the CS process (i.e., spray direction, nozzle speed, and spray distance) can be precisely controlled to achieve uniform coating on the target surface. All these features could enhance the industrial applicability of the proposed route for 3D-printed polymer electronics.

Besides its intrinsic advantages, however, one important limitation of this approach could be its low patterning resolution. Although the described approach is effective for large-area metallization on polymers even with curvilinear geometries, it cannot directly fabricate high-resolution (i.e., submillimeter) conductive metallization on 3D-printed parts without a shadow mask. The reason is the size restriction of the CS nozzle (i.e., nozzle exit diameter \approx 5 mm), which could limit the use of this approach in such applications, requiring high spatial resolution like microelectronics. On the other hand, as illustrated in Figure 11, conductive metallization with

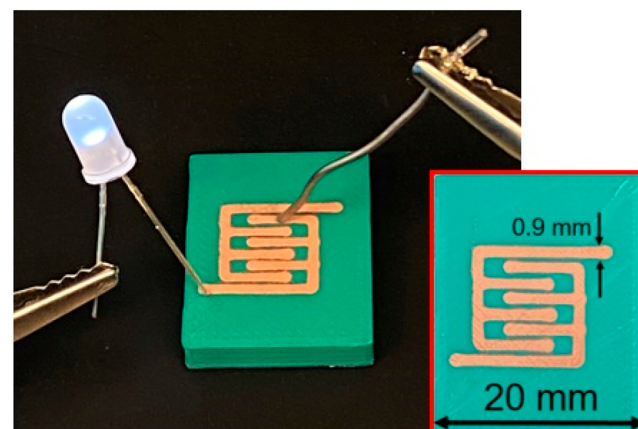


Figure 11. Conductively metallized 3D-printed ABS part with submillimeter resolution.

submillimeter resolution (i.e., \approx 0.9 mm line width) can be achieved by masking, which would also enlarge the application areas of the proposed metallization route in a scalable manner.

Another drawback of the proposed method is its limitation in processing complicated 3D architectures with inner structures. In detail, CS cannot ensure the deposition of the functional particles into the intricate structures, thereby limiting its use in complicated 3D parts. Except for these limitations, the proposed hybrid metallization approach ensures high-throughput and cost-effective metallization on 3D-printed freeform polymers without the need of acid etching and palladium seeding, thereby promising a green alternative for polymer electronics manufacturing.

CONCLUSION

An additive surface metallization route that sequentially comprises (1) material extrusion 3D printing, (2) CS metallization, and (3) electroless deposition (ED) was

employed for electrically conductive metallization on 3D-printed parts. Polymer substrates, namely, ABS and PLA, were accurately produced by using material extrusion-based 3D printing. The micrometer-sized Cu particles were then deposited on the as-printed polymer surfaces by CS, and further utilized as the catalytic side for the ED process. The subsequent ED ensured a highly conductive metal film on the as-CS polymer surface. The following conclusions can be drawn from the present study:

- Unlike the traditional polymer metallization methods, the CS-assisted ED does not require any acid etching, cost-intensive palladium seeding, vacuum, and precursor; thereby it is an environmental-friendly approach.
- The resulting metallization on the polymer surfaces exhibited promising electrical conductivity (i.e., 6.47×10^6 S m⁻¹ for ABS and 5.27×10^6 S m⁻¹ for PLA parts) as compared to traditional polymer metallization methods that involve acid etching, palladium seeding, and 3D printing with conductive filaments.
- Curvilinear-shaped polymer structures were effectively metallized owing to the multiaxis compatibility of the CS process. The developed parts show a similar performance.
- Fabricated electronic circuits including a conductive puzzle and LED circuit on freeform curvilinear-shaped surfaces demonstrated the effectiveness of the proposed approach.
- Using a shadow mask, functional metallization with submillimeter (i.e., ≈ 0.9 mm line width) resolution was achieved on the 3D-printed parts.
- The established additive surface metallization route reveals great potential for rapid custom prototyping of functionally metallized polymers in consumer electronics, energy harvesting, automotive, defense, and many more.

ASSOCIATED CONTENT

Supporting Information

The Supporting Information is available free of charge at <https://pubs.acs.org/doi/10.1021/acsaclm.3c00893>.

IR camera image of the cold spray nozzle; additional SEM images of the as-cold sprayed and overplated polymer surfaces and interfaces; surface roughness test setup; description of the cross-cut adhesion test procedure and characterization results; schematic of the pull-off adhesion test; brief description of the pull-off test procedure and adhesive strength results ([PDF](#))

AUTHOR INFORMATION

Corresponding Authors

Semih Akin – School of Mechanical Engineering, Purdue University, West Lafayette, Indiana 47907, United States; orcid.org/0000-0002-3644-7133; Email: sakin@purdue.edu

Martin Byung-Guk Jun – School of Mechanical Engineering and Indiana Manufacturing Competitiveness Center (IN-MaC), Purdue University, West Lafayette, Indiana 47907, United States; orcid.org/0000-0002-0512-7209; Email: mbgjun@purdue.edu

Author

Chandra Nath – School of Mechanical Engineering, Purdue University, West Lafayette, Indiana 47907, United States

Complete contact information is available at:
<https://pubs.acs.org/10.1021/acsaclm.3c00893>

Author Contributions

S.A.: conceptualization, formal analysis, design, investigation, experiments, characterization, visualization, data curation, writing original-draft, review and editing. C.N.: conceptualization, review and editing. M.B.J.: conceptualization, resources, review and editing. All authors commented on the manuscript.

Notes

The authors declare no competing financial interest.

ACKNOWLEDGMENTS

The authors thank Dr. Taehoo Chang for his help with microstructure analysis.

NOMENCLATURE

Symbol Description

A	area
L	length
R	resistance
R/R ₀	relative resistance
S	siemens
ρ	resistivity
Ω	ohm

Abbreviations Description

ABS	acrylonitrile–butadiene–styrene
AM	additive manufacturing
CS	cold spray
as-CS	as-cold sprayed
Cu	copper
CA	contact angle
EDX	energy-dispersive X-ray
ED	electroless deposition
ITO	indium tin oxide
ITO-PET	ITO-coated poly(ethylene terephthalate)
ITO-PEN	ITO-coated poly(ethylene naphthalate)
Pd	palladium
PLA	poly(lactic acid)
SEM	scanning electron microscopy
OM	optical microscopy
XRD	X-ray diffraction
3D	three-dimensional

REFERENCES

- (1) Melentiev, R.; Yudhanto, A.; Tao, R.; Vuchkov, T.; Lubineau, G. Metallization of Polymers and Composites: State-of-the-Art Approaches. *Mater. Des.* **2022**, *221*, 110958.
- (2) Zhang, J.; Feng, J.; Jia, L.; Zhang, H.; Zhang, G.; Sun, S.; Zhou, T. Laser-Induced Selective Metallization on Polymer Substrates Using Organocopper for Portable Electronics. *ACS Appl. Mater. Interfaces* **2019**, *11* (14), 13714–13723.
- (3) Cai, J.; Lv, C.; Watanabe, A. Laser Direct Writing and Selective Metallization of Metallic Circuits for Integrated Wireless Devices. *ACS Appl. Mater. Interfaces* **2018**, *10* (1), 915–924.
- (4) Kim, M. J.; Cruz, M. A.; Ye, S.; Gray, A. L.; Smith, G. L.; Lazarus, N.; Walker, C. J.; Sigmarsson, H. H.; Wiley, B. J. One-Step Electrodeposition of Copper on Conductive 3D Printed Objects. *Addit. Manuf.* **2019**, *27*, 318–326.

- (5) Horiuchi, S.; Fujita, T.; Hayakawa, T.; Nakao, Y. Micro-patterning of Metal Nanoparticles via UV Photolithography. *Adv. Mater.* **2003**, *15* (17), 1449–1452.
- (6) Romani, A.; Mantelli, A.; Tralli, P.; Turri, S.; Levi, M.; Suriano, R. Metallization of Thermoplastic Polymers and Composites 3D Printed by Fused Filament Fabrication. *Technologies* **2021**, *9* (3), 49.
- (7) He, P.; Cao, J.; Ding, H.; Liu, C.; Neilson, J.; Li, Z.; Kinloch, I. A.; Derby, B. Screen-Printing of a Highly Conductive Graphene Ink for Flexible Printed Electronics. *ACS Appl. Mater. Interfaces* **2019**, *11* (35), 32225–32234.
- (8) Roach, D. J.; Roberts, C.; Wong, J.; Kuang, X.; Kovitz, J.; Zhang, Q.; Spence, T. G.; Qi, H. J. Surface Modification of Fused Filament Fabrication (FFF) 3D Printed Substrates by Inkjet Printing Polyimide for Printed Electronics. *Addit. Manuf.* **2020**, *36*, 101544.
- (9) Tian, X.; Lee, P. M.; Tan, Y. J.; Wu, T. L. Y.; Yao, H.; Zhang, M.; Li, Z.; Ng, K. A.; Tee, B. C. K.; Ho, J. S. Wireless Body Sensor Networks Based on Metamaterial Textiles. *Nat. Electron.* **2019**, *2* (6), 243–251.
- (10) Akin, S.; Gabor, T.; Jo, S.; Joe, H.; Tsai, J. T.; Park, Y.; Lee, C. H.; Park, M. S.; Jun, M. B. G. Dual Regime Spray Deposition Based Laser Direct Writing of Metal Patterns on Polymer Substrates. *J. Micro Nano-Manufacturing* **2020**, DOI: 10.1115/1.4046282.
- (11) Angel, K.; Tsang, H. H.; Bedair, S. S.; Smith, G. L.; Lazarus, N. Selective Electroplating of 3D Printed Parts. *Addit. Manuf.* **2018**, *20*, 164–172.
- (12) Flowers, P. F.; Reyes, C.; Ye, S.; Kim, M. J.; Wiley, B. J. 3D Printing Electronic Components and Circuits with Conductive Thermoplastic Filament. *Addit. Manuf.* **2017**, *18*, 156–163.
- (13) Zhan, J.; Tamura, T.; Li, X.; Ma, Z.; Sone, M.; Yoshino, M.; Umezawa, S.; Sato, H. Metal-Plastic Hybrid 3D Printing Using Catalyst-Loaded Filament and Electroless Plating. *Addit. Manuf.* **2020**, *36*, 101556.
- (14) Perera, A. T. K.; Wu, K.; Wan, W. Y.; Song, K.; Meng, X.; Umezawa, S.; Wang, Y.; Sato, H. Modified Polymer 3D Printing Enables the Formation of Functionalized Micro-Metallic Architectures. *Addit. Manuf.* **2023**, *61*, 103317.
- (15) Gerges, T.; Semet, V.; Lombard, P.; Allard, B.; Cabrera, M. Rapid 3D-Plastronics Prototyping by Selective Metallization of 3D Printed Parts. *Addit. Manuf.* **2023**, *73*, 103673.
- (16) Kirleis, M. A.; Simonson, D.; Charipar, N. A.; Kim, H.; Charipar, K. M.; Auyeung, R. C. Y.; Mathews, S. A.; Piqué, A. Laser Embedding Electronics on 3D Printed Objects. In *Laser 3D Manufacturing*; SPIE: 2014; Vol. 8970, p 897004.
- (17) Liu, F.; Xie, D.; Jiao, C.; Bai, D.; Wu, H.; Shen, L.; Tian, Z.; Zhao, J. Selective Metallization on Additive Manufactured Polymer for Fabrication of Integrated Device. *J. Mater. Sci.* **2022**, *57* (2), 1506–1515.
- (18) Tang, X.; Bi, C.; Han, C.; Zhang, B. A New Palladium-Free Surface Activation Process for Ni Electroless Plating on ABS Plastic. *Mater. Lett.* **2009**, *63* (11), 840–842.
- (19) Ahn, J.; Sim, H. H.; Kim, J. H.; Wajahat, M.; Kim, J. H.; Bae, J.; Kim, S.; Pyo, J.; Jeon, C. J.; Kim, B. S.; Baek, S. H.; Seol, S. K. Air-Pressure-Assisted Pen-Nib Printing for 3D Printed Electronics. *Adv. Mater. Technol.* **2022**, *7* (6), 2101172.
- (20) Azar, G. T. P.; Danilova, S.; Krishnan, L.; Fedutik, Y.; Cobley, A. J. Selective Electroless Copper Plating of Ink-Jet Printed Textiles Using a Copper-Silver Nanoparticle Catalyst. *Polymers (Basel)* **2022**, *14* (17), 3467.
- (21) Yin, S.; Cavaliere, P.; Aldwell, B.; Jenkins, R.; Liao, H.; Li, W.; Lupoi, R. Cold Spray Additive Manufacturing and Repair: Fundamentals and Applications. *Addit. Manuf.* **2018**, *21* (April), 628–650.
- (22) Liberati, A. C.; Che, H.; Fallah, P.; Vo, P.; Yue, S. Pull-off Testing and Electrical Conductivity of Sn-Based Metal Powder Mixtures Cold Sprayed on Carbon Fiber-Reinforced Polymers. *Journal of Thermal Spray Technology* **2022**, *31*, 1792–1812.
- (23) Che, H.; Liberati, A. C.; Chu, X.; Chen, M.; Nobari, A.; Vo, P.; Yue, S. Metallization of Polymers by Cold Spraying with Low Melting Point Powders. *Surf. Coat. Technol.* **2021**, *418*, 127229.
- (24) Gärtner, F.; Schmidt, T.; Stoltenhoff, T.; Kreye, H. Recent Developments and Potential Applications of Cold Spraying. *Adv. Eng. Mater.* **2006**, *8* (7), 611–618.
- (25) Melentiev, R.; Yu, N.; Lubineau, G. Polymer Metallization via Cold Spray Additive Manufacturing: A Review of Process Control, Coating Qualities, and Prospective Applications. In *Additive Manufacturing*; Elsevier: 2021; p 102459.
- (26) Ganeshan, A.; Yamada, M.; Fukumoto, M. Cold Spray Coating Deposition Mechanism on the Thermoplastic and Thermosetting Polymer Substrates. *J. Therm. Spray Technol.* **2013**, *22* (8), 1275–1282.
- (27) Akin, S.; Tsai, J. T.; Park, M. S.; Jeong, Y. H.; Jun, M. B. G. Fabrication of Electrically Conductive Patterns on Acrylonitrile-Butadiene-Styrene Polymer Using Low-Pressure Cold Spray and Electroless Plating. *J. Micro Nano-Manufacturing* **2020**, DOI: 10.1115/1.4049578.
- (28) Tsai, J.-T.; Akin, S.; Zhou, F.; Park, M. S.; Bahr, D. F.; Jun, M. B.-G. Electrically Conductive Metallized Polymers by Cold Spray and Co-Electroless Deposition. *ASME Open J. Eng.* **2022**, *1*.
- (29) Cano-Vicent, A.; Tambuwala, M. M.; Hassan, S. S.; Barh, D.; Aljabali, A. A. A.; Birkett, M.; Arjunan, A.; Serrano-Aroca, Á. Fused Deposition Modelling: Current Status, Methodology, Applications and Future Prospects. In *Additive Manufacturing*; Elsevier: 2021; p 102378.
- (30) Olivera, S.; Muralidhara, H. B.; Venkatesh, K.; Gopalakrishna, K.; Vivek, C. S. Plating on Acrylonitrile-Butadiene-Styrene (ABS) Plastic: A Review. *J. Mater. Sci.* **2016**, *51*, 3657–3674.
- (31) Milovanovic, S.; Pajnik, J.; Lukic, I. Tailoring of Advanced Poly(Lactic Acid)-Based Materials: A Review. *J. Appl. Polym. Sci.* **2022**, *139*, 51839.
- (32) Silver/silver chloride (60/40) paste for screen printing, Sigma-Aldrich. <https://www.sigmapellic.com/US/en/product/aldrich/901773> (accessed 2023-06-26).
- (33) CenterLine Supersonic Spray Technology - SST Cold Spray Applications and Coating Use. <https://www.supersonicspray.com/products/sst-powders> (accessed 2023-08-04).
- (34) Akin, S.; Wu, P.; Tsai, J.-T.; Nath, C.; Chen, J.; Jun, M. B.-G. A Study on Droplets Dispersion and Deposition Characteristics under Supersonic Spray Flow for Nanomaterial Coating Applications. *Surf. Coat. Technol.* **2021**, *426*, 127788.
- (35) Akin, S.; Jo, S.; Jun, M. B. G. A Cold Spray-Based Novel Manufacturing Route for Flexible Electronics. *J. Manuf. Process.* **2023**, *86*, 98–108.
- (36) Prashar, G.; Vasudev, H. A Comprehensive Review on Sustainable Cold Spray Additive Manufacturing: State of the Art, Challenges and Future Challenges. *J. Clean. Prod.* **2021**, *310*, 127606.
- (37) Akin, S.; Lee, S.; Jo, S.; Ruzgar, D. G.; Subramaniam, K.; Tsai, J.-T.; Jun, M. B.-G. Cold Spray-Based Rapid and Scalable Production of Printed Flexible Electronics. *Addit. Manuf.* **2022**, *60*, 103244.
- (38) Choi, H.; Lee, J. G.; Mai, X. D.; Beard, M. C.; Yoon, S. S.; Jeong, S. Supersonically Spray-Coated Colloidal Quantum Dot Ink Solar Cells. *Sci. Rep.* **2017**, *7* (1), 1–8.
- (39) Gillet, V.; Aubignat, E.; Costil, S.; Courant, B.; Langlade, C.; Casari, P.; Knapp, W.; Planche, M. P. Development of Low Pressure Cold Sprayed Copper Coatings on Carbon Fiber Reinforced Polymer (CFRP). *Surf. Coat. Technol.* **2019**, *364*, 306–316.
- (40) Fallah, P.; Rajagopalan, S.; McDonald, A.; Yue, S. Development of Hybrid Metallic Coatings on Carbon Fiber-Reinforced Polymers (CFRPs) by Cold Spray Deposition of Copper-Assisted Copper Electroplating Process. *Surf. Coat. Technol.* **2020**, *400*, 126231.
- (41) Ghosh, S. Electroless Copper Deposition: A Critical Review. *Thin Solid Films* **2019**, *669*, 641–658.
- (42) Jo, S.; Akin, S.; Park, M. S.; Jun, M. B. G. Selective Metallization on Glass Surface by Laser Direct Writing Combined with Supersonic Particle Deposition. *Manuf. Lett.* **2022**, *31*, 64–68.
- (43) Chang, T.; Akin, S.; Kim, M. K.; Murray, L.; Kim, B.; Cho, S.; Huh, S.; Teke, S.; Couetil, L.; Jun, M. B.-G.; Lee, C. H. Programmable Dual Regime Spray for Large-Scale and Custom-Designed Electronic Textiles. *Adv. Mater.* **2022**, *34*, 2108021.

- (44) Hebbar, R. S.; Isloor, A. M.; Ismail, A. F. Contact Angle Measurements. *Membr. Charact.* **2017**, *219–255*.
- (45) Seok, S.; Park, H. D.; Kim, J. Characterization and Analysis of Metal Adhesion to Parylene Polymer Substrate Using Scotch Tape Test for Peripheral Neural Probe. *Micromachines* **2020**, *11* (6), *605*.
- (46) ASTM International. D3359-17 (2017). Standard Test Methods for Rating Adhesion by Tape Test. (ASTM Int. West Conshohocken, PA, 2020) **2021**, *1–9*.
- (47) ASTM. D4541-09: Standard Test Method for Pull-Off Strength of Coatings Using Portable Adhesion. *ASTM Int.* **2014**, *1–16*.
- (48) Che, H.; Chu, X.; Vo, P.; Yue, S. Metallization of Various Polymers by Cold Spray. *J. Therm. Spray Technol.* **2018**, *27* (1–2), *169–178*.
- (49) Fan, Z.; Gao, J.; Wu, Y.; Yin, D.; Chen, S.; Tu, H.; Wei, T.; Zhang, C.; Zhu, H.; Jin, H. Highly Enhanced Mechanical, Thermal, and Crystallization Performance of PLA/PBS Composite by Glass Fiber Coupling Agent Modification. *Polymers (Basel)* **2023**, *15* (15), *3164*.
- (50) Rodríguez-Panes, A.; Claver, J.; Camacho, A. M. The Influence of Manufacturing Parameters on the Mechanical Behaviour of PLA and ABS Pieces Manufactured by FDM: A Comparative Analysis. *Materials (Basel)* **2018**, *11* (8), *1333*.
- (51) 3D Printer Filaments, Sindoh 3D Printer, Unmistakable Sindoh. <https://3dprinter.sindoh.com/materials/filaments#3dwox1> (accessed 2022-05-23).
- (52) Che, H.; Liberati, A. C.; Chu, X.; Chen, M.; Nobari, A.; Vo, P.; Yue, S. Metallization of Polymers by Cold Spraying with Low Melting Point Powders. *Surf. Coat. Technol.* **2021**, *418*, *127229*.
- (53) Che, H.; Vo, P.; Yue, S. Metallization of Carbon Fibre Reinforced Polymers by Cold Spray. *Surf. Coat. Technol.* **2017**, *313*, *236–247*.
- (54) Gibas, A.; Baszczuk, A.; Jasiorowski, M.; Winnicki, M. Prospects of Low-Pressure Cold Spray for Superhydrophobic Coatings. *Coatings* **2019**, *9* (12), *829*.
- (55) Wenzel, R. N. Resistance of Solid Surfaces to Wetting by Water. *Ind. Eng. Chem.* **1936**, *28* (8), *988–994*.
- (56) Clavijo, C. E.; Crockett, J.; Maynes, D. Hydrodynamics of Droplet Impingement on Hot Surfaces of Varying Wettability. *Int. J. Heat Mass Transfer* **2017**, *108*, *1714–1726*.
- (57) Guo, D.; Kazasidis, M.; Hawkins, A.; Fan, N.; Leclerc, Z.; MacDonald, D.; Nastic, A.; Nikbakht, R.; Ortiz-Fernandez, R.; Rahmati, S.; Razavipour, M.; Richer, P.; Yin, S.; Lupoi, R.; Jodoin, B. Cold Spray: Over 30 Years of Development Toward a Hot Future. *J. Therm. Spray Technol.* **2022**, *31* (4), *866–907*.
- (58) Cui, X.; Hutt, D. A.; Conway, P. P. Evolution of Microstructure and Electrical Conductivity of Electroless Copper Deposits on a Glass Substrate. *Thin Solid Films* **2012**, *S20* (19), *6095–6099*.
- (59) Augustin, A.; Rajendra Udupa, K.; Udaya Bhat, K. Effect of Coating Current Density on the Wettability of Electrodeposited Copper Thin Film on Aluminum Substrate. *Perspect. Sci.* **2016**, *8*, *472–474*.
- (60) Amini, M.; Bayrami, A.; Marashi, M. N.; Arab, A.; Ellern, A.; Woo, L. K. Synthesis, Structure, and Catalytic Properties of Copper, Palladium and Cobalt Complexes Containing an N,O-Type Bidentate Thiazoline Ligand. *Inorg. Chim. Acta* **2016**, *443*, *22–27*.
- (61) Kakanuru, P.; Pochiraju, K. Moisture Ingress and Degradation of Additively Manufactured PLA, ABS and PLA/SiC Composite Parts. *Addit. Manuf.* **2020**, *36*, *101529*.
- (62) Zhang, Y.; Zhang, T.; Shi, H.; Liu, Q.; Shi, Y.; Wang, T. Electroless Plating Cycle Process for High-Conductivity Flexible Printed Circuits. *ACS Sustain. Chem. Eng.* **2021**, *9* (35), *11991–12004*.
- (63) Melentiev, R.; Tao, R.; Fatta, L.; Tevtia, A. K.; Verghese, N.; Lubineau, G. Towards Decoupling Chemical and Mechanical Adhesion at the Electroplated Metal/Polymer Interface via Precision Surface Texturing. *Surfaces and Interfaces* **2023**, *38*, *102875*.
- (64) Han, B.; Peng, Q.; Li, R.; Rong, Q.; Ding, Y.; Akinoglu, E. M.; Wu, X.; Wang, X.; Lu, X.; Wang, Q.; Zhou, G.; Liu, J.-M.; Ren, Z.; Giersig, M.; Herczynski, A.; Kempa, K.; Gao, J. Optimization of Hierarchical Structure and Nanoscale-Enabled Plasmonic Refraction for Window Electrodes in Photovoltaics. *Nat. Commun.* **2016**, *7* (1), *1–8*.
- (65) Hutasoit, N.; Topa, S. H.; Javed, M. A.; Rahman Rashid, R. A.; Palombo, E.; Palanisamy, S. Antibacterial Efficacy of Cold-Sprayed Copper Coatings against Gram-Positive *Staphylococcus Aureus* and Gram-Negative *Escherichia Coli*. *Materials* **2021**, *14* (22), *6744*.
- (66) Saha, D. C.; Boegel, S. J.; Tanvir, S.; Nogueira, C. L.; Aucoin, M. G.; Anderson, W. A.; Jahed, H. Antiviral and Antibacterial Cold Spray Coating Application on Rubber Substrate, Disruption in Disease Transmission Chain. *J. Therm. Spray Technol.* **2023**, *32*, *818–830*.
- (67) ASTM D3359: Measuring Adhesion by Tape Test, Standard Test Methods For 2009. <https://www.astm.org/DATABASE.CART/HISTORICAL/D3359-02.htm> (accessed 2021-10-20).
- (68) Sahoo, S. K.; Sahu, A. K.; Mahapatra, S. S. Environmental Friendly Electroless Copper Metallization on FDM Build ABS Parts. *Int. J. Plast. Technol.* **2017**, *21* (2), *297–312*.
- (69) Li, D.; Yang, C. L. Acidic Electroless Copper Deposition on Aluminim-Seeded ABS Plastics. *Surf. Coat. Technol.* **2009**, *203* (23), *3559–3568*.
- (70) Ryspayeva, A.; Jones, T. D. A.; Khan, S. R.; Esfahani, M. N.; Shuttleworth, M. P.; Harris, R. A.; Kay, R. W.; Desmulliez, M. P. Y.; Marques-Hueso, J. Selective Metallization of 3D Printable Thermoplastic Polyurethanes. *IEEE Access* **2019**, *7*, *104947–104955*.
- (71) Goo, Y.-S.; Lee, Y.-I.; Kim, N.; Lee, K.-J.; Yoo, B.; Hong, S.-J.; Kim, J.-D.; Choa, Y.-H. Ink-Jet Printing of Cu Conductive Ink on Flexible Substrate Modified by Oxygen Plasma Treatment. *Surf. Coat. Technol.* **2010**, *205*, *S369–S372*.
- (72) Potts, S. J.; Korochkina, T.; Holder, A.; Jewell, E.; Phillips, C.; Claypole, T. The Influence of Carbon Morphologies and Concentrations on the Rheology and Electrical Performance of Screen-Printed Carbon Pastes. *J. Mater. Sci.* **2022**, *57* (4), *2650–2666*.
- (73) Im, S. G.; Gleason, K. K. Systematic Control of the Electrical Conductivity of Poly(3,4-Ethylenedioxythiophene) via Oxidative Chemical Vapor Deposition. *Macromolecules* **2007**, *40* (18), *6552–6556*.
- (74) Ratautas, K.; Vosylius, V.; Jagminienė, A.; Stankevičienė, I.; Norkus, E.; Račiukaitis, G. Laser-Induced Selective Electroless Plating on PC/ABS Polymer: Minimization of Thermal Effects for Supreme Processing Speed. *Polymers* **2020**, *12* (10), *2427*.
- (75) Rahimi, R.; Ochoa, M.; Ziae, B. Direct Laser Writing of Porous-Carbon/Silver Nanocomposite for Flexible Electronics. *ACS Appl. Mater. Interfaces* **2016**, *8* (26), *16907–16913*.
- (76) Sigma-Aldrich. <https://www.sigmadlrich.com/US/en>.